

Poster

📅 Thu. Jul 31, 2025 6:00 PM - 7:00 PM JST | Thu. Jul 31, 2025 9:00 AM - 10:00 AM UTC 🏛️ Poster (2F The Salon) (2F The Salon)

[P] Poster session2

6:00 PM - 7:00 PM JST | 9:00 AM - 10:00 AM UTC

[3P27]

Plasma modification of single walled carbon nanohorns by using different gases

*Artur P. Terzyk¹ (1. Nicolaus Copernicus University (Poland))

6:00 PM - 7:00 PM JST | 9:00 AM - 10:00 AM UTC

[3P28]

High-Entropy Alloy Nanoparticle Catalysts Synthesized by Flash Lamp Annealing for Ethanol Oxidation Reaction

*Peng Zhou¹, Mai Thanh Nguyen², Tetsu Yonezawa² (1. School of Engineering, Hokkaido University (Japan), 2. Faculty of Engineering, Hokkaido University (Japan))

6:00 PM - 7:00 PM JST | 9:00 AM - 10:00 AM UTC

[3P29]

Design of Catalytically Active MnO_x Species for Ammoxidation Reaction by Heat Treatment of Mn–Al Layered Double Hydroxide

*Shiori Arai¹, Takayoshi Hara¹, Nobuyuki Ichikuni¹ (1. Department of Applied Chemistry and Biotechnology Graduate School of Engineering, Chiba University (Japan))

6:00 PM - 7:00 PM JST | 9:00 AM - 10:00 AM UTC

[3P30]

Insight into Structural Change of Ni(II)-Al(III) Layered Double Hydroxide under Heat Treatment: Design of NiO-Al₂O₃ Nanocomposite Catalysts toward Hydrogen Transfer Reaction of Furfural

*Tsugumi Kato¹, Takayoshi Hara¹, Nobuyuki Ichikuni¹ (1. Department of Applied Chemistry and Biotechnology, Division of Advanced Science and Engineering, Graduate School of Science and Engineering, Chiba University (Japan))

6:00 PM - 7:00 PM JST | 9:00 AM - 10:00 AM UTC

[3P31]

Design of Various Anions-intercalated Layered Ytterbium Hydroxide as a Solid Base Catalyst for the Knoevenagel Reaction in Water

*Yuko Kinoshita¹, Takayoshi Hara¹, Nobuyuki Ichikuni¹ (1. Department of Applied Chemistry and Biotechnology, Graduate School of Engineering, Chiba University (Japan))

6:00 PM - 7:00 PM JST | 9:00 AM - 10:00 AM UTC

[3P32]

Surface modification of Polyester Textiles with Clay Nanosheets for Adsorption of Waste Models

*Mitsutaka Watanabe¹, Hisanao Usami¹, Moto Suzuki² (1. Department of Textile Science and Technology, Graduateschool of Science and Technology, Shinshu University (Japan), 2. hap corporation (Japan))

6:00 PM - 7:00 PM JST | 9:00 AM - 10:00 AM UTC

[3P33]

Heterostructure of MoTi-MXene and ZnCr LDH hybrid obtained by in-situ crystal growth of LDH on MXene for potential photocatalyst

*Farhan Hadi¹, Jae-Min OH¹ (1. Dongguk University (Korea))

6:00 PM - 7:00 PM JST | 9:00 AM - 10:00 AM UTC

[3P34]

Particle morphology controlled Ni-Co hydroxide synthesized via sol-gel method for efficient and stable oxygen evolution reaction

*Jaeseong Kim¹, Jae-Min Oh¹ (1. Dongguk University (Korea))

6:00 PM - 7:00 PM JST | 9:00 AM - 10:00 AM UTC

[3P35]

Stabilisation of iron-oxo dimers in a natural layered clay for efficient photocatalysts comparable to TiO₂

*Hamza ElHosainy El-Hosainy^{1,2}, Ezz-Elregal Ezz-Elregal³, Shinichiro Takano⁴, Yusuke Ide^{1,3}, Tomohiko Okada⁴ (1. National Institute for Materials Science (Japan), 2. Institute of Nanoscience and Nanotechnology, Kafrelsheikh University (Egypt), 3. Graduate School of Engineering Science, Yokohama National University (Japan), 4. Department of Materials Chemistry, Faculty of Engineering, Shinshu University (Japan))

6:00 PM - 7:00 PM JST | 9:00 AM - 10:00 AM UTC

[3P36]

Stabilization of molecular TiO₄ species on the pore surface of mesoporous silica and its photocatalytic properties

*Masashi Morita¹, Hikaru Inada¹, Kazuyuki Maeda¹ (1. Tokyo University of Agriculture and Technology (Japan))

6:00 PM - 7:00 PM JST | 9:00 AM - 10:00 AM UTC

[3P37]

Fabrication of porous complex oxide objects by 3D printing and the thermal conversion of metal hydroxide acrylate nanoparticles.

*Yudai Inada¹, Naoki Tarutani¹, Miki Asanome¹, Sota Shimizu², Yasuaki Tokudome², Hiroki Yamada³, Toshiaki Ina³, Seiya Shimono³, Kiyofumi Katagiri¹, Kei Inumaru¹ (1. Hiroshima University (Japan), 2. Osaka Metropolitan University (Japan), 3. Japan Synchrotron Radiation Research Institute (Japan))

6:00 PM - 7:00 PM JST | 9:00 AM - 10:00 AM UTC

[3P38]

Investigation of dispersion behavior of Ni-Al LDH nanoparticles in solvents

*Takuya Mori¹, Yosuke Ando¹, Shin-ichi Takeda², Ai Takabatake³, Naoki Tarutani⁴, Atsushi Nakahira¹, Yasuaki Tokudome¹ (1. Osaka Metropolitan University (Japan), 2. Takeda Colloid Techno Consulting (Japan), 3. MS Scientific. (Japan), 4. Hiroshima University (Japan))

6:00 PM - 7:00 PM JST | 9:00 AM - 10:00 AM UTC

[3P39]

Investigation of liquid-phase synthesis conditions toward morphology control of nickel hydroxide salt nanoparticles

*Keiichiro Tsujimoto¹, Naoki Tarutani¹, Kiyofumi Katagiri¹, Kei Inumaru¹ (1. Hiroshima university (Japan))

6:00 PM - 7:00 PM JST | 9:00 AM - 10:00 AM UTC

[3P40]

Thermal conversion of nickel hydroxide acrylate nanoparticles immobilized on TiO₂ for photocatalytic H₂ production.

*Rei Nitomakida¹, Naoki Tarutani¹, Kiyofumi Katagiri¹, Kei Inumaru¹, Sayako Inoue², Hiroki Yamada³, Toshiaki Ina³ (1. Hiroshima University (Japan), 2. Ehime University (Japan), 3. Japan Synchrotron Radiation Research Institute (Japan))

6:00 PM - 7:00 PM JST | 9:00 AM - 10:00 AM UTC

[3P41]

Investigation of the Unique Co-catalytic Function of AlB₂ in Photocatalytic Overall Water Splitting

*Ryuichi Yamaguchi¹, Atsushi Anzai¹, Shoma Matsubara¹, Shota Tsunewaki¹, Naoki Tarutani¹, Kiyofumi Katagiri¹, Kei Inumaru¹ (1. Hiroshima University (Japan))

6:00 PM - 7:00 PM JST | 9:00 AM - 10:00 AM UTC

[3P42]

Nanoparticle Monolayer Films of Metal Hydroxide Acrylates toward Efficient Electrocatalysts

*Miki Asanome¹, Naoki Tarutani¹, Kiyofumi Katagiri¹, Kei Inumaru¹, Toshiaki Ina², Hiroki Yamada², Koji Kimoto³, Oki Saito⁴, Kenji Okada⁴, Masahide Takahashi⁴ (1. Hiroshima Univ. (Japan), 2. JASRI (Japan), 3. NIMS (Japan), 4. OMU (Japan))

6:00 PM - 7:00 PM JST | 9:00 AM - 10:00 AM UTC

[3P43]

Higher excited-state dynamics of perylene monoimide coordinated to inorganic nanocrystals

*Mizuki Sato¹, Daisuke Yoshioka¹, Yuki Nagai¹, Yoichi Kobayashi^{1,2} (1. Ritsumeikan Univ. (Japan), 2. PREST JST (Japan))

6:00 PM - 7:00 PM JST | 9:00 AM - 10:00 AM UTC

[3P44]

Visible light-induced decomposition of perfluoroalkyl substances by CdS/ZnS core/shell nanocrystals

*Kohki Tanaka¹, Yuki Nagai¹, Yoichi Kobayashi^{1,2} (1. Ritsumeikan Univ. (Japan), 2. PREST, JST (Japan))

6:00 PM - 7:00 PM JST | 9:00 AM - 10:00 AM UTC

[3P45]

Electron density distribution analysis of Mn-As layered compounds with different types of antiferromagnet

*Kentaro Katayama¹, Chikako Moriyoshi¹, Kouichi Takase² (1. Hiroshima University (Japan), 2. Nihon University (Japan))

6:00 PM - 7:00 PM JST | 9:00 AM - 10:00 AM UTC

[3P46]

The effect of charge density on the crystal structure of layered double hydroxides of the Ni-Al type containing carbonate or chloride ions

*Kota Nakanishi¹, Chikako Moriyoshi¹, Shogo Kawaguchi², Ryo Sasai³ (1. Hiroshima University (Japan), 2. JASRI (Japan), 3. Shimane University (Japan))

6:00 PM - 7:00 PM JST | 9:00 AM - 10:00 AM UTC

[3P47]

QENS study on local dynamics of hydration water using Si311 analyzer

*Takeshi Yamada¹ (1. CROSS (Japan))

6:00 PM - 7:00 PM JST | 9:00 AM - 10:00 AM UTC

[3P48]

Trace blood detection by inducing fluorescence of hemoglobin
via selective iron exclusion

*Yoon Kang¹, Jae-Min Oh¹ (1. Dongguk university (Korea))

6:00 PM - 7:00 PM JST | 9:00 AM - 10:00 AM UTC

[3P49]

Anisotropic growth of layered double hydroxides on planar aluminum or spherical alumina
substrates

*Taeho Kim¹, Yoon Kang¹, Jaeseong Kim¹, Rena Oi², Shota Mochizuki², Ryoto Kobayashi²,
Tomohiko Okada², Jae-Min Oh¹ (1. Dongguk University (Korea), 2. Shinshu University (Japan))

6:00 PM - 7:00 PM JST | 9:00 AM - 10:00 AM UTC

[3P50]

Hybridization of a Zn-smectite with spherical silica particles

*Shota Mochizuki¹, Tomohiko Okada¹ (1. Graduate School of Science and Technology, Shinshu
University (Japan))

6:00 PM - 7:00 PM JST | 9:00 AM - 10:00 AM UTC

[3P51]

Adsorption of Anionic Red Dyes on Smectite in the Presence of Multivalent Cations

*Rena Oi¹, Tomohiko Okada¹ (1. Graduate School of Science and Technology, Shinshu
University (Japan))

6:00 PM - 7:00 PM JST | 9:00 AM - 10:00 AM UTC

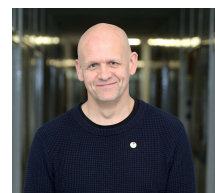
[3P52]

Formation of Titania Particles via Incorporation of Titanium (IV) Oxyacetylacetonate into
Mesoporous Silica

*Kakeru Taniuchi¹, Tomohiko Okada¹, Masashi Morita² (1. Graduated School of Science and
Technology, Shinshu University (Japan), 2. Tokyo University of Agriculture and Technology
(Japan))

Zahira Bano, Artur P. Terzyk,

Faculty of Chemistry, Physicochemistry of Carbon Materials
Research Group, Nicolaus Copernicus University in Toruń, Gagarin
Street 7, 87-100 Toruń, Poland
E-mail: aterzyk@chem.umk.pl




Plasma modification of single walled carbon nanohorns by using different gases

In this study, the surface of single-walled carbon nanohorns (SWCNHs) was modified using plasma at different gaseous environments, i.e. air, argon, and ammonia. The influence of various parameters including treatment time, gas flow rate, and plasma power was systematically investigated to assess their effect on the internal structure and surface chemistry of the SWCNHs. Effect of a gas and plasma treatment on the surface properties, porosity and the structure of SWCNHs were investigated by using different techniques. Transmission Electron Microscopy was employed to observe morphological and microstructural changes, zeta potential and Dynamic light scattering (DLS) measurements were used to identify the formation of surface groups, while Dynamic Light Scattering was utilized to assess the hydrodynamic diameter and dispersion behavior. The open structures of modified SWCNHs will be used to produce new anti-icing sponges. The approach aims to enhance durability and reduce maintenance costs by minimizing ice accretion.

Keywords: SWCNs, Plasma treatment, Anti-icing, Superhydrophobic, Carbon nanohorn

We gratefully acknowledge the financial support from NCN Opus 22 project: UMO-2021/43/B/ST5/00421. And European Union in the framework of the project ‘Young Universities for the Future of Europe’ – a post-doc program, agreement no. 101081327) and Polish Ministry of Science and Higher Education within the framework of the program titled "International Co-Financed Projects" (agreement no. 5678/HE/2023/2024/2).

Peng Zhou ¹ , Mai Thanh Nguyen ² , Tetsu Yonezawa ²	
Graduate School of Engineering, Hokkaido University ¹ , Faculty of Engineering, Hokkaido University ² E-mail: peng.zhou.u5@elms.hokudai.ac.jp (Peng Zhou), tetsu@eng.hokudai.ac.jp (Tetsu Yonezawa)	
High-Entropy Alloy Nanoparticle Catalysts Synthesized by Flash Lamp Annealing for Ethanol Oxidation Reaction	
<p>High entropy alloys (HEAs) typically composed of five or more metals with near-equimolar ratios, exhibit stabilized heterogeneous crystalline solid-solution phase due to their high mixing entropy. HEA nanoparticles (HEA-NPs) offer advantages such as compositional versatility, enhanced corrosion resistance, and synergistic catalytic activity. In this study, we synthesized Rh-Pd-Ir-Pt HEA-NPs using flash lamp annealing, a method that provides high heating and cooling rates to facilitate the formation of HEAs in a non-equilibrium state. This method also enables the single step production of HEA-NPs as catalysts on support substrates like graphene oxide.</p> <p>XRD and STEM analyses confirmed the successful synthesis of HEA-NPs, and STEM-EDS mapping revealed a uniform distribution of metal elements within the nanoparticles. Particle sizes were controlled by adjusting the synthesis conditions. The formation mechanism involves the reduction of metal chlorides to metal atoms or clusters (monomers) at high temperatures, followed by nucleation and growth into HEA-NPs.</p> <p>The synthesized HEA-NPs were evaluated as catalysts for the ethanol oxidation reaction (EOR), a complex process requiring multiple active sites with different functions for dehydrogenation to acetaldehyde, C-C bond splitting, and oxidation of C1 fragments. Our findings demonstrate that these Pt-group HEA-NPs are high catalytic activity for EOR.</p>	

Shiori Arai, Takayoshi Hara*, and Nobuyuki Ichikuni

Department of Applied Chemistry and Biotechnology

Graduate School of Engineering, Chiba University

E-mail: t_hara@faculty.chiba-u.jp (Takayoshi Hara)



Design of Catalytically Active MnO_x Species for Ammoxidation Reaction
by Heat Treatment of Mn–Al Layered Double Hydroxide

In this study, a nitrate-intercalated layered Mn^{2+} - Al^{3+} double hydroxide ($\text{Mn}^{2+}/\text{Al}^{3+}=2$, $\text{NO}_3^-/\text{Mn}_2\text{Al}$ LDH) was synthesized according to the previous report.[1] The LDH_cal_T K catalyst was obtained by the temperature-programmed heat treatment (10 K/min) under air, and the synthesized catalyst was applied to the ammoxidation reaction of benzaldehyde to benzonitrile in the presence of atmospheric O_2 . [2] Based on the temperature-programmed synchrotron XRD (*tp*-SXRD), TG-DTA (Fig. 1), and in-situ Mn K-edge XANES (Fig. 2) under the same heating rate, the collapse of layered structure (up to 473 K) and decomposition of hydroxide nanosheets (from 473 K to 523 K) were clearly observed.

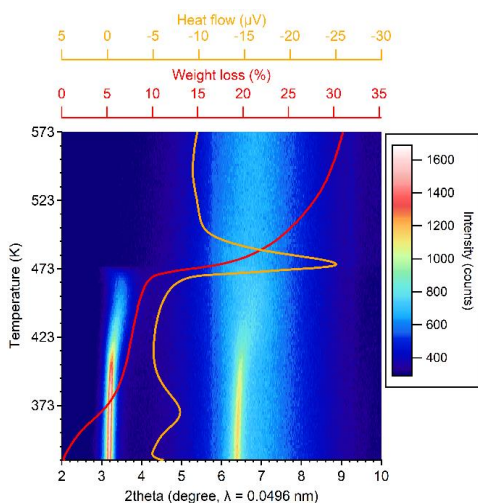


Fig. 1 2D mapping of *tp*-SXRD and TG-DTA data of $\text{NO}_3^-/\text{Mn}_2\text{Al}$ LDH.

The LDH_cal_573 K catalyst exhibited high catalytic activity in the ammoxidation reaction. A finely dispersed Mn_3O_4 species, identified as the main crystalline phase by XRD, is likely to play a crucial role in the catalytic reaction.

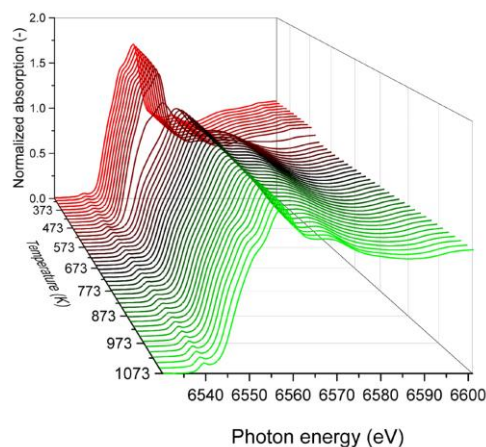


Fig. 2 In-situ Mn K-edge XANES of $\text{NO}_3^-/\text{Mn}_2\text{Al}$ LDH.

[1] S. Aisawa, *et al.*, *J. Solid State Chem.*, **2002**, 167, 152.

[2] T. Hara, *et al.*, *Solv. Extr. Ion Exch.*, **2025**, 43, 94.

Tsugumi Kato, Takayoshi Hara*, Nobuyuki Ichikuni

Department of Applied Chemistry and Biotechnology, Graduate
School of Engineering, Chiba University

E-mail: t_hara@faculty.chiba-u.jp (Takayoshi Hara)



Insight into Structural Change of Ni(II)-Al(III) Layered Double Hydroxide under Heat Treatment: Design of NiO-Al₂O₃ Nanocomposite Catalysts toward Hydrogen Transfer Reaction of Furfural

In this study, a Ni₂AlO_*T* catalyst derived from the calcination at *T* K of CO₃²⁻/Ni₂Al LDH, obtained by the hydrothermal method using urea,[1] was synthesized. To clarify the structural change of CO₃²⁻/Ni₂Al LDH during calcination, temperature-programmed synchrotron XRD, TG-DTA, and Ni K-edge XANES (Fig. 1) were obtained under the same heating conditions (rate: 10 K/min). XRD data revealed the Ni₂AlO_*T* catalyst (*T* ≥ 673 K) was mainly composed of small sized NiO species and amorphous Al₂O₃. In addition, the decomposition of the hydroxide nanosheets into NiO species around 653 K was also confirmed. The Ni₂AlO_*T* catalysts were applied to hydrogen transfer reaction of furfural with 2-propanol (Table 1). The yield of furfuryl alcohol increased with increasing calcination temperature. From the H₂-TPR measurements, it was found that a highly stable NiO species against the reduction into Ni(0) was generated on the Ni₂AlO_*T* matrix by the calcination at high temperature.

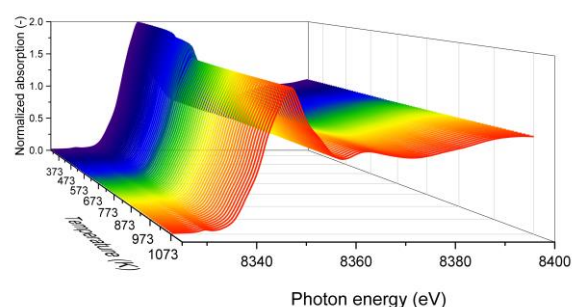


Fig. 1 Normalized Ni K-edge XANES for the CO₃²⁻/Ni₂Al LDH as a function of temperature programmed calcination (10 K/min) under air flow

Table 1. Results of hydrogen transfer reaction of furfural with 2-propanol^a

<chem>c1ccoc1C=O</chem> + <chem>CC(C)O</chem> $\xrightarrow[393\text{ K, 3 h}]{\text{Catalyst (0.1 g)}}$ <chem>c1ccoc1CO</chem> + <chem>CC(C)=O</chem>			
Entry	Catalyst	Conv. (%) ^b	Yield (%) ^b
1	Blank	-	<i>n.d.</i>
2	NiO	10	<i>n.d.</i>
3	Ni ₂ AlO_673	35	35
4	Ni ₂ AlO_773	32	32
5	Ni ₂ AlO_873	44	44
6	Ni ₂ AlO_973	43	43
7	Ni ₂ AlO_1073	45	45
8	Ni ₂ AlO_1173	51	51

^aCatalyst (0.1 g), furfural (1 mmol), 2-propanol (5 mL), 373 K, 3 h. ^bDetermined by GC using internal standard technique.

1) R. Sasai, *et al.*, *Bull. Chem. Soc. Jpn.*, 95, 802-812 (2022).

Yuko Kinoshita, Takayoshi Hara,* and Nobuyuki Ichikuni

Your Photo



Department of Applied Chemistry and Biotechnology,
Graduate School of Engineering, Chiba University
E-mail: t_hara@faculty.chiba-u.jp (Takayoshi Hara)

Design of Various Anions-intercalated Layered Ytterbium Hydroxide as a Solid Base Catalyst for the Knoevenagel Reaction in Water

We have already reported the Knoevenagel reaction in water with an acetate-intercalated Layered Yttrium Hydroxide ($\text{AcO}^-/\text{Y-LRH}$) as a solid base catalyst. The $\text{AcO}^-/\text{Y-LRH}$ catalyst showed the lift-up behavior by the formation of acetate-water composite in the interlayer.[1] To create more effective solid catalyst toward Knoevenagel condensation in aqueous phase, a Layered Rare-earth Hydroxide (LRH) consisting of heavy Rare-earth element should be selected, because of their strong Lewis acidity. In this work, various anions-intercalated Layered Ytterbium Hydroxide (Yb-LRH) catalysts were synthesized and applied into Knoevenagel reaction between ethyl cyanoacetate (**1**) and benzaldehyde (**2**) in water. Although changing the interlayer anion may cause the interlayer distance (d_{00l}) of Yb-LRH, the d_{00l} did not shift in water as shown in **Table 1**. As expected, a replacement of Y to Yb in LRH catalyst showed the higher activity (entries 1 and 2). Among the Yb-LRH catalyst with various interlayer anion was tested (**Table 1**), the $\text{AcO}^-/\text{Yb-LRH}$ showed the highest catalytic activity with TON of 7.0, compared with that of $\text{AcO}^-/\text{Y-LRH}$ (entries 1 and 2). In the case of the Yb-LRH catalysts with narrow d_{00l} spacing, the reaction rate was slow (entries 3, 5 and 6). Moreover, the $\text{C}_3\text{H}_7\text{COO}^-/\text{Yb-LRH}$ catalysts that have more extended interlayer space did not efficiently promote this reaction (entry 4).

[1] T. Hara *et al.*, *Catal. Sci. Technol.*, **2022**, 12, 2061.

Table 1. Knoevenagel condensation in water^a

$\text{CH}_2=\text{C}(\text{CN})\text{CO}_2\text{Et} + \text{PhCHO} \xrightarrow[\text{H}_2\text{O}, 323 \text{ K}, 1 \text{ h}]{\text{LRH catalyst}} \text{PhCH}=\text{C}(\text{CN})\text{CO}_2\text{Et} + \text{H}_2\text{O}$				
Entry	Catalyst	d_{00l} (nm) ^b	Yield (%) ^c	TON (-) ^d
1	$\text{AcO}^-/\text{Yb-LRH}$	1.28	77	7.0
2	$\text{AcO}^-/\text{Y-LRH}$	1.30	>99	3.9
3	$\text{NO}_3^-/\text{Yb-LRH}$	0.87	62	4.4
4	$\text{C}_3\text{H}_7\text{COO}^-/\text{Yb-LRH}$	1.60	64	3.9
5	$\text{Cl}^-/\text{Yb-LRH}$	0.84	45	2.4
6	$\text{Br}^-/\text{Yb-LRH}$	0.80	19	0.9

^a LRH catalyst (0.05 g), **1** (1.5 mmol), **2** (1 mmol), H_2O (5 mL), 323 K, 1 h. ^b Calculated from XRD data. ^c Determined by GC using an internal standard technique. ^d Based on Yb^{3+} or Y^{3+} amount.

Mitsutaka Watanabe¹, Hisanao Usami¹, Moto Suzuki²

Shinshu University¹, hap corporation²

E-mail: 24fs473a@shinshu-ac.jp (Watanabe Mitsutaka)

hisayan@shinshu-u.ac.jp (Hisanao Usami)



Surface modification of Polyester Textiles with Clay Nanosheets for Adsorption of Waste Models

Polyester textiles were modified with clay nanosheets as adsorption layers on the most outer surface of the textiles and fibers. Adsorption of cationic and anionic waste on the modified polyester textiles and cleaning process with pure water without detergents were studied. Alkylamines, aliphatic acids and ionic dyes were selected as cationic and anionic model stains, respectively.

Original PET textiles surface was modified to be cationic with polyethylenimine (PEI). Then, sodium montmorillonite (MMT, composed of anionic nanosheets) was adsorbed on the cationic PET surface electrostatically, resulting in multilayers of MMT by controlling the concentration of MMT solution.

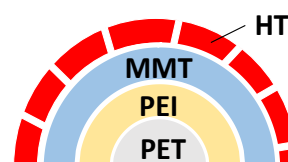


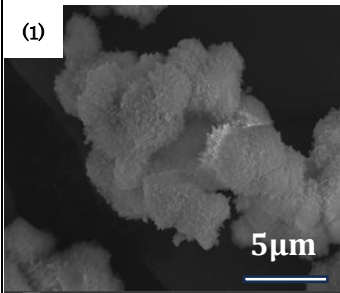
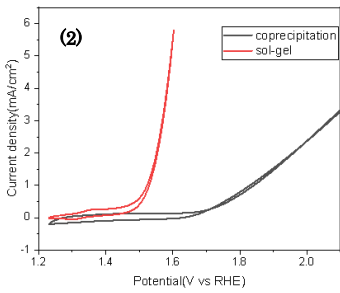


Fig. 1 Schematic model of HT-PET

Hydrotalcite (HT, composed of cationic nanosheets) layer was deposited electrostatically on the MMT surface to form the multi-coated PET fiber as shown in Fig. 1. The layered structure was characterized by SEM, ATR-FTIR spectroscopy and zeta potential measurement. Amount of adsorption of amines and acids were measured by titration. Adsorption of the ionic dyes were quantified by diffuse reflectance absorption spectroscopy.

The amount of adsorption of ammonia and butylamine was 400 μmol for MMT-PET. It is contrasted that the untreated PET and PEI-modified PET shows small amount of adsorption less than 100 μmol . The value is greater than the amount of adsorption estimated based on the anionic charge density of MMT nanosheet, suggesting a type of multilayered deposition. Dyes were also absorbed on the HT-PET. However, only 10 % of the adsorbed dyes were removed by washing with tap water without detergent. The reason was speculated that most of the dyes were penetrated through the adsorption layers and deposited on the pristine PET surface by a hydrophobic interaction.

Farhan Hadi	
Affiliation E-mail: hadifarhan851@gmail.com (Farhan Hadi), jaemin.oh@dongguk.edu (Jae-Min OH)	
Heterostructure of MoTi-MXene and ZnCr-LDH hybrid obtained by in-situ crystal growth of LDH on MXene for potential photocatalyst	
<p>In this study, a heterostructure hybrid consisting of Mo₂TiC₂T_x MXene and ZnCr layered double hydroxide (LDH) was synthesized via an in-situ hydrothermal assisted crystal growth. In the hybrid, the Mo₂TiC₂T_x nanosheets would provide a conductive and chemically active substrate for the nucleation promoting uniform growth of ZnCr LDH nanoplates on the MXene layer, resulting in a well-integrated heterostructure. Structural analysis using X-ray diffraction (XRD) confirmed the coexistence of both MXene and LDH phases in a super-lattice manner; transmission electron microscopy (TEM) corroborated tight interfacial contact as well as a consistent layered morphology, suggesting strong heterojunction formation. Optical properties of the composite evaluated by solid-state UV–Vis diffuse reflectance spectroscopy (UV–Vis DRS), and the Tauc plot showed a bandgap energy of approximately 1.60 eV. This narrow bandgap indicates that the MoTi-MXene/ZnCr-LDH hybrid is photoactive under visible light, which is highly desirable for photocatalytic applications. The structural configuration is expected to promote efficient charge separation and transfer across the MXene–LDH interface, enhancing the degradation of organic pollutants under illumination. The combination of layered morphology, strong interfacial contact, and visible-light-responsive bandgap strongly supports the potential of this composite as a high-performance photocatalyst for environmental remediation.</p>	

<div>Jaeseong Kim</div> <div>E-mail: jasonk214@naver.com</div> <div>jaemin.oh@dongguk.edu (corresponding, Jae-Min Oh)</div>		
<div>Particle morphology controlled Ni-Co hydroxide synthesized via sol-gel method for efficient and stable oxygen evolution reaction</div> <div>Secondary particle morphology-controlled Ni-based hydroxide/oxide was synthesized via phase-separation assisted sol-gel methods for oxygen evolution reaction (OER) catalysts. According to the X-ray diffraction pattern, the sol-gel synthesized Ni(OH)₂ had alpha phase whereas the conventionally precipitated one possessed beta phase possibly due to the different water accessibility during the reaction. The scanning electron microscopy revealed that the sol-gel synthesized Ni-hydroxide had sea urchin like primary particle with average secondary particle size of 2 μm with high homogeneity; while the conventionally precipitated Ni(OH)₂ had undefined morphology with serious agglomeration. The well-ordered hierarchy in the particle arrangement was corroborated with the N₂ adsorption-desorption isotherm, in which sol-gel sample exhibited dramatically higher specific surface area of 182 m²/g than that of conventional one (71 m²/g). It was expected that the well-defined primary particle and high specific surface area facilitated proton donor-acceptor on the surface, thereby improving OER activity as well as leading to improved ion exchange efficiency and reduced overpotential. Similarly, Ni-Co binary hydroxide was synthesized on Ni foam substrate via a sol-gel method, enabling as an OER catalyst in a binder free manner. This approach provides high electrochemical activity and excellent structural stability. Furthermore, phase-separating agent during synthesis-controlled particles, offering advantage in microstructural tuning.</div>		
<div><div><div>(1)</div></div><div><div>(2)</div></div></div>	<div>Figure 1. Sea urchin like sol-gel synthesized Ni-hydroxide primary particle</div> <div>Figure 2. NiCo hydroxide OER activity between via sol-gel and coprecipitation method .</div>	

Hamza El-Hosainy

Affiliation: National Institute for Materials Science

E-mail: Elhosainy.Hamza@nims.go.jp, IDE.Yusuke@nims.go.jp,
tomohiko@shinshu-u.ac.jp



Stabilisation of iron-oxo dimers in a natural layered clay for efficient photocatalysts comparable to TiO₂

Because solid photocatalysis is a (potentially) feasible means of tackling environmental and energy issues, research into even a pioneering solid photocatalyst, TiO₂, is still growing. In addition, the development of solid photocatalysts alternative to TiO₂ has been burgeoning due to its cost-ineffectiveness, environmental and health concerns.^{1,2} A ultimate alternative to TiO₂ is naturally-occurring photocatalysts; however, few reports have demonstrated natural materials showing photocatalytic activities higher than or comparable to that of TiO₂. Here, we report a simple method to stabilise otherwise fleeting iron(III)-oxo dimers by intercalating them into the interlayer space of a natural layered clay.³ Comprehensive analyses and calculations reveal that the Fe³⁺-oxo dimers are stabilized via direct coordination to the silicate layers, with sufficient interlayer void space for reactant accessibility. The resulting material exhibits an excellent photocatalytic activity toward the oxidation of formic acid in water and formaldehyde in air comparable to the benchmark TiO₂ (P25) photocatalyst. This approach offers a sustainable pathway to design efficient, earth-abundant, and structurally tunable photocatalysts.

- 1) Ide, Y., Tominaka, S., Yoneno, Y., Komaguchi, K., Takei, T., Nishida, H., Tsunoji, N., Machida, A., and Sano, T., *Chem. Sci.*, **10**, 6604 (2019).
- 2) El-Hosainy, H., Mine, S., Toyao, T., Shimizu, K.-I., Tsunoji, N., Esmat, M., Doustkhah, E., El-Kemary, M., and Ide, Y., *Mater. Today Nano*, **19**, 100227 (2022).
- 3) El-Hosainy, H., Ezz-Elregal E. M., Takano, S., Miyakage, T., Chen, D., He, C., Toyao, T. Shimizu K.-I., Ide, Y. and Okada, T., *Chem. Commun.*, **61**, 5435 (2025).

Masashi Morita, Hikaru Inada and Kazuyuki Maeda

Department of Applied Chemistry, Graduate School of Engineering,
Tokyo University of Agriculture and Technology, 2-24-16 Naka-
cho, Koganei, Tokyo 184-8588, Japan.

E-mail: m-morita@go.tuat.ac.jp




Stabilization of molecular TiO_4 species on the pore surface of mesoporous silica and its photocatalytic properties

Although molecular tetrahedral Ti-oxo species exhibit unique electronic and photochemical properties due to their discrete energy levels,¹ which are different from those of anatase and rutile, such Ti-oxo species are generally unstable and readily transformed to amorphous/crystalline TiO_2 (bulk phases, nanoparticles, and clusters) via hydrolysis and condensation. Here, molecular Ti-oxo species were immobilized on the pore surface of mesoporous silica SBA-15 by grafting titanium(IV) oxyacetylacetonate using the surface silanol groups of SBA-15 as a scaffold, followed by chemical etching with dilute hydrochloric acid to form molecular TiO_4 species.² These Ti species mainly exist as isolated tetrahedrally coordinated structures, as was confirmed by diffuse reflectance UV-vis and Raman spectroscopy. The SBA-15-immobilized molecular TiO_4 exhibited higher photocatalytic activity than the reference photocatalysts (P25 and Ti-MCM-41) for both H_2 production from methanol solution and CO_2 reduction to C_2 products such as ethanol and acetic acid.

References:

- [1] H. Yamashita, K. Mori, Y. Kuwahara, T. Kamegawa, M. Wen, P. Verma and M. Che, *Chem. Soc. Rev.*, **47**, 8072 (2018).
- [2] H. Inada, M. Morita and K. Maeda, *Dalton Trans.*, 53, 13756 (2024).

Yudai Inada, Naoki Tarutani, Miki Asanome, Sota Shimizu, Yasuaki Tokudome, Hiroki Yamada, Toshiaki Ina, Seiya Shimonono, Kiyofumi Katagiri, and Kei Inumaru	Your Photo 
Affiliation: Hiroshima University, OMU, JASRI E-mail: inadayudai@hiroshima-u.ac.jp (Yudai Inada), n-tarutani@hiroshima-u.ac.jp (Naoki Tarutani)	
Fabrication of porous complex oxide objects by 3D printing and the thermal conversion of metal hydroxide acrylate nanoparticles.	
<p>Photopolymerization-based 3D printing has emerged as a transformative manufacturing strategy for fabricating complex architectures with tunable functionalities. In particular, nano/microscale porous architectures are of significant interest due to their high surface area and enhanced mass transport properties. Despite considerable research efforts, 3D printing of porous structures consist of ceramics remains a major challenge. We demonstrated that highly concentrated dispersions of Ni hydroxide acrylate (Ni-HA) nanoparticles enable fabrication of complex objects via 3D printing¹⁾. Subsequent heat-treatment successfully converts the printed objects into oxides with microscale porosity. In this study, we focus on the introduction and control of porous structures in transition metal oxides through 3D printing using nanoparticle dispersions.</p> <p>Metal hydroxide acrylate nanoparticle dispersed in N,N-dimethylformamide were prepared through a previously reported method. 3D printing was carried out with the prepared dispersions by adding photoinitiators. The printed objects were heat-treated at 400–900 °C under argon atmosphere, followed by heat-treatment under air flow.</p> <p>Gyroid shaped objects having millimeter-scale pores were successfully printed by using CoNi-HA nanoparticle dispersions. The printed objects were heat-treated under argon atmosphere. As shown in Fig. 1a, scanning electron microscopy (SEM) images of the cross-section of heat-treated objects revealed a nanoscale phase-separated morphology with domain size of ~20 nm. Based on Raman spectroscopy and X-ray diffraction analysis, these domains were identified as Co–Ni alloy and carbon. Subsequent heat-treatment in an air atmosphere resulted in the formation of a continuous porous structure composed of (Co,Ni)O with an average pore diameter of 45 nm (Fig. 1b). The porous structure could be tuned by adjusting the heat-treatment conditions, while preserving the original printed shapes. This solid–solid phase separation process enables the formation of hierarchical porosity without sacrificial templates.</p> <p>1) N. Tarutani, <i>et al.</i>, <i>J. Ceram. Soc. Jpn.</i> 131, 830–836 (2023).</p>	

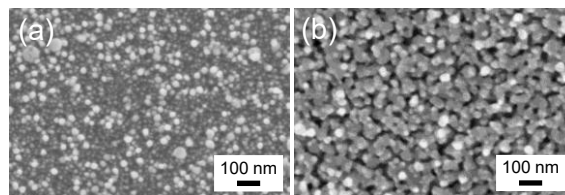



Fig. 1 Cross-section SEM images of printed objects after heat treatment at (a) 600 °C under argon atmosphere and (b) subsequently 600 °C in air atmosphere.

Takuya Mori	
Affiliation: Osaka Metropolitan Univ. E-mail: sn24908r@st.omu.ac.jp	
Investigation of dispersion behavior of Ni-Al LDH nanoparticles in solvents	

Colloidal nanoparticles are crucial in various applications. In particular, high-solid-concentration aqueous and water-miscible colloidal nanoparticles have become increasingly important to meet the requirement of low environmental impact. To date, our research group has reported the synthesis of layered double hydroxide (LDH) and layered hydroxide salts (LHSs) nanoparticles that exhibit dispersion at high concentration in solvents (~10 wt%)[1]. Especially, NiAl LDH nanoparticles was found to exhibit extremely high dispersibility in alcohol solvents at a concentration of 40 wt%. It is suggested that the origin of this high dispersibility and dispersion stability lies in the formation of high-density solvation layers on the surface of LDH nanoparticles [2]. In this study, we investigated the properties of solvents and surface of these LDH nanoparticles comprising the dispersion to gain further insights into this dispersibility.

The dispersibility of LDH nanoparticles strongly depends on the solvent type. Despite their comparable polarities (and Hansen solubility parameters), significant difference in dispersibility was observed for the cases methanol and ethylene glycol solvents employed. Furthermore, no clear correlation was observed among the type of ligand used to modify the LDH nanoparticles, zeta potential of nanoparticles, and dispersibility of LDH nanoparticles in solvents. The measurement of density of dispersion revealed that the density of the solvent phase in the dispersion increased with increasing particle concentration in the methanol. In contrast, in the ethylene glycol system, the density of the solvent phase in the dispersion remained unchanged even as particle concentration increased. These results support the fact that the high-density solvent-layering on the surface of LDH nanoparticles contributes to the dispersion stability of the particles in the solvent.

[1] Y. Tokudome, *J. Ceram. Soc. Jpn.*, 125, 587, (2017).
[2] Y. Tokudome, et al., *Langmuir*, 41, 8545, (2025).

Keiichiro Tsujimoto, Naoki Tarutani, Kiyofumi Katagiri,
Kei Inumaru

Affiliation: Hiroshima University
E-mail: m252950@hiroshima-u.ac.jp (Keiichiro Tsujimoto),
n-tarutani@hiroshima-u.ac.jp (Naoki Tarutani)



Investigation of liquid-phase synthesis conditions toward morphology control of nickel hydroxide salt nanoparticles

Transition metal-based layered hydroxides are recognized as promising catalysts for efficient oxygen evolution reactions. Since the discovery of the excellent electrocatalytic performance of exfoliated hydroxide nanosheets, extensive research has been devoted to the synthesis and catalytic application of hydroxide nanosheets and nanoparticles. Recent simulation and experimental studies have revealed that the edge regions exhibit higher electrocatalytic activity than the inner regions, highlighting the importance of morphological control of metal hydroxides for the development of optimized catalysts. Our group has developed a method for synthesizing well-dispersed metal hydroxide salt nanoparticles with diameters below 10 nm¹⁾. In this study, we focus on the morphological tuning of these nanoparticles. The effects of synthetic parameters, including reaction temperature, solvents, precursor concentration, and base reagents, are systematically investigated in relation to particle size, morphology, and dispersibility.

Nickel hydroxide acrylate nanoparticles were synthesized according to a previously reported method¹⁾. During the synthesis, reaction temperature, solvent type, precursor concentration, and base reagents were systematically varied. The obtained nanoparticles were characterized by X-ray diffraction (XRD), small-angle X-ray scattering (SAXS), dynamic light scattering, and infrared spectroscopy.

Figure 1 shows the XRD patterns of samples synthesized at different temperatures. Samples prepared at lower temperatures exhibited a small peak below $2\theta = 10^\circ$, corresponding to the 003 diffraction of the layered structure. In contrast, a clear 110 diffraction peak was detected, implying the formation of two-dimensional plate-like morphology. As the reaction temperature increased, the 003 peaks became more prominent, indicating growth along the stacking direction. These results suggest that the crystal growth of layered nickel hydroxide salts proceeds rapidly in the lateral direction and slowly along the stacking direction. This trend was supported by fractal dimension analysis based on SAXS measurement. Solvent type and precursor concentration had a minor influence on the morphology, whereas specific base reagents promoted lateral growth of the particles.

1) N. Tarutani *et al.*, *ACS Mater. Lett.*, **4**, 1430 (2022).

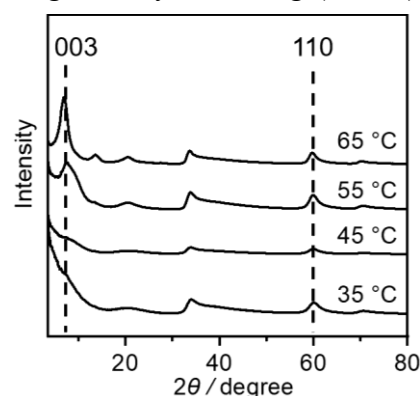



Fig. 1. XRD patterns of nickel hydroxide acrylates synthesized at reaction temperatures ranging from 35 °C to 65 °C.

Rei Nitomakida, Naoki Tarutani, Kiyofumi Katagiri, Kei Inumaru, Sayako Inoue, Hiroki Yamada, Toshiaki Ina	
Affiliation Hiroshima University, Ehime University, JASRI E-mail: nitorei2100@hiroshima-u.ac.jp (Rei Nitomakida), n-tarutani@hiroshima-u.ac.jp (Naoki Tarutani)	

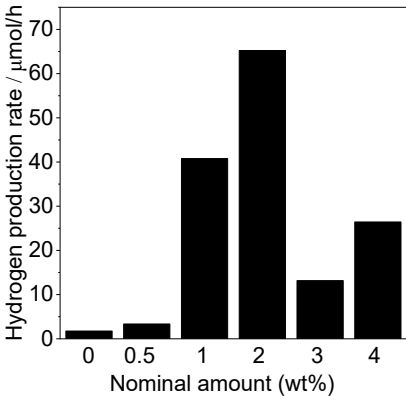
Thermal conversion of nickel hydroxide acrylate nanoparticles immobilized on TiO₂ for photocatalytic H₂ production.

Photocatalytic water splitting is a promising technology for environmentally friendly hydrogen production. In addition to the development of photocatalysts, designing efficient and noble-metal-free cocatalysts is essential to achieve high catalytic activity. However, the design of such cocatalyst remains challenging due to the size requirement, typically below 10 nm. In our previous study, it was demonstrated that heat-treatment of nickel hydroxide salt nanoparticles (<10 nm) leads to conversion to metals and various inorganic compounds¹⁾. In this study, we applied this thermal conversion approach to develop TiO₂-based photocatalysts loaded with Ni-based compound cocatalysts.

Dispersions of Ni hydroxide acrylate (NHA) nanoparticles were obtained by adding propylene oxide to an ethanoic solution containing NiCl₂·6H₂O and acrylic acid. Rutile TiO₂ nanoparticles were suspended in the NHA nanoparticle dispersions. After drying, the collected powders were heat-treated at 600°C in an argon atmosphere to obtain Ni-based cocatalyst-loaded TiO₂. For comparison, a control sample was prepared by following the same procedure using Ni(NO₃)₂ aqueous solution instead of NHA nanoparticle dispersions.

Transmission electron microscopy revealed that pristine TiO₂ nanoparticles, with a size of ~35 nm, exhibited distinct surface lattice fringes. After immobilization of NHA nanoparticles followed by heat-treatment, the particle retained a similar size, however, surface amorphous layers approximately 2–3 nm thick were partially observed. This suggests interaction between TiO₂ and NHA-derived species. Ni species formed after heat-treatment were identified as Ni@NiO_x-like composite based on X-ray absorption near-edge structure and X-ray photoelectron spectroscopy. Photocatalytic water splitting tests under ultraviolet light irradiation with a sacrificial agent showed that Ni(NO₃)₂-loaded samples were inactive. In contrast, NHA-loaded samples exhibited enhanced performance. The activity increased with Ni loading, reaching a H₂ evolution rate ~37 times higher than that of pristine TiO₂ at a Ni content of 2 wt% (Fig. 1).

1) N. Tarutani *et al.*, *Nanoscale*, **15**, 15656, (2023).



Nominal amount (wt%)	Hydrogen production rate / μmol/h
0	2
0.5	4
1	41
2	65
3	13
4	27

Fig. 1. Rate of H₂ evolution by Ni@NiO_x-loaded TiO₂ under ultraviolet light irradiation. The aqueous solutions contain 10 vol % of methanol.

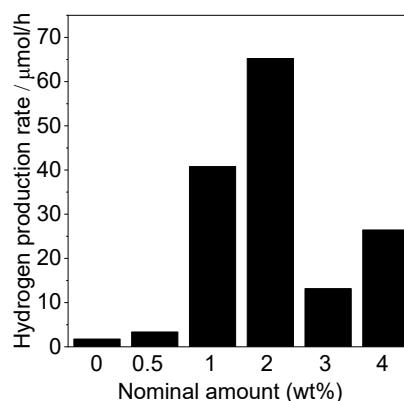


Fig. 1. Rate of H₂ evolution by Ni@NiO_x-loaded TiO₂ under ultraviolet light irradiation. The aqueous solutions contain 10 vol % of methanol.

R. Yamaguchi, A. Anzai, S. Matsubara, S. Tsunewaki,
N. Tarutani, K. Katagiri, and K. Inumaru

Affiliation : Hiroshima University.

E-mail: r-yamaguchi@hiroshima-u.ac.jp (R. Yamaguchi),

inumaru@hiroshima-u.ac.jp (K. Inumaru)



Investigation of the Unique Co-catalytic Function of AlB_2 in Photocatalytic Overall Water Splitting

Effective co-catalysts are crucial for enhancing the activity of water splitting photocatalysts. While metals and transition metal oxides are commonly utilized as co-catalysts, we discovered that the intermetallic compound AlB_2 also functions as a cocatalyst. We demonstrated that AlB_2 powder improves the activity of the **KCaSrTa₅O₁₅ (KCSTO)** photocatalyst through simple mechanical mixing. In this study, we investigated how the synthesis conditions, composition, and loading amounts of AlB_2 affect its co-catalytic activity.

We synthesized **KCSTO** by solid-state reaction. AlB_2 was prepared by solid-state reaction of a mixture of elemental Al and B powders in evacuated sealed quartz tubes. For **Sample 1**, a mixture (Al:B = 1:2) was heated at 900 °C for 4 h. For **Sample 2**, a mixture (Al:B = 1.3:2) was heated at 900 °C for 3 h, followed by slow cooling from 900 °C to 800 °C over 1 h. These AlB_2 samples were then mechanically mixed with **KCSTO**. Photocatalytic activity was measured using an internal irradiation flow cell with a 400 W high-pressure Hg lamp.

According to X-ray diffraction patterns (**Fig. 1a**), **Sample 1** contained a considerable amount of AlB_{12} , with only a minor byproduct of $\alpha\text{-Al}_2\text{O}_3$. For **Sample 2**, the formation of AlB_{12} was almost suppressed. Photocatalytic measurements with these **AlB_2 -KCSTO** composites (**Fig. 1b**) confirmed that overall water splitting occurred in all cases, exhibiting a stoichiometric H_2 : O_2 ratio of 2:1. **Sample 1** showed ca. 3 times higher activity compared to pristine **KCSTO**. Notably, **Sample 2** achieved the highest photocatalytic activity. In conclusion, by adjustments of the raw material composition and temperature profiles during AlB_2 synthesis could prevent byproduct AlB_{12} formation and consequently achieve a high co-catalytic performance.

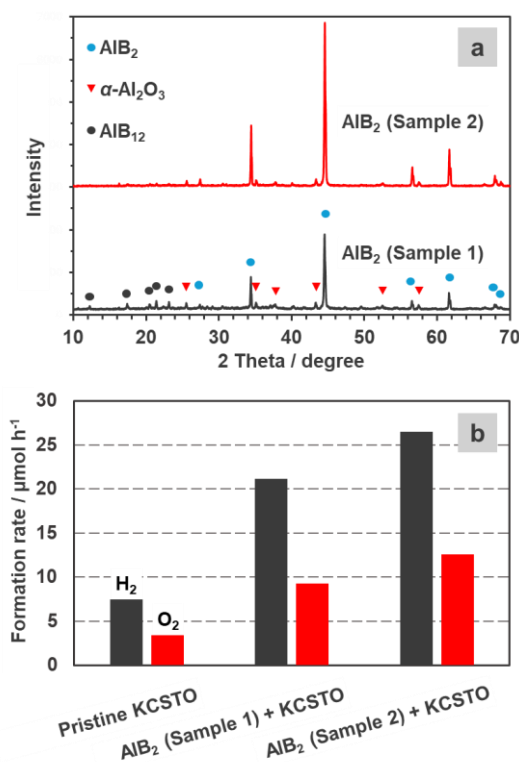
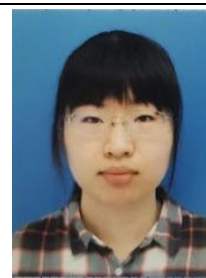


Fig. 1 XRD patterns of AlB_2 (a) and photocatalytic activity results using these samples (b).

Miki Asanome, Naoki Tarutani, Kiyofumi Katagiri, Kei Inumaru, Toshiaki Ina, Hiroki Yamada, Koji Kimoto, Oki Saito, Kenji Okada, Masahide Takahashi

Affiliation: Hiroshima Univ., JASRI, NIMS, OMU

E-mail: m-asanome@hiroshima-u.ac.jp (Miki Asanome),
n-tarutani@hiroshima-u.ac.jp (Naoki Tarutani)



Nanoparticle Monolayer Films of Metal Hydroxide Acrylates toward Efficient Electrocatalysts

Layered transition metal hydroxides are recognized as potential low-cost catalysts for efficient oxygen evolution reaction. Typically, hydroxide catalysts are co-dispersed with conductive additives and binder materials, followed by drying to prepare electrodes for electrochemical characterization. However, this conventional method results in randomly aggregated catalysts, which hinders the systematic understanding of catalyst structure–activity relationships and the development of rational design strategies. In this study, we developed nanoparticle monolayer films through a self-assembly process using metal hydroxide salts nanoparticles.

Nickel-based metal hydroxide acrylate (Ni-MHA) nanoparticles were synthesized by epoxide-mediated basification¹⁾. Molecule-modified Au electrodes were dipped in the nanoparticle dispersions to trigger self-assembly and immobilization of nanoparticles. Structural characterization and electrochemical measurements were carried out using the same procedure with different types of Au electrodes.

Ni-MHA nanoparticles, with an average diameter of 1.7 nm, were successfully synthesized. Au electrodes were immersed in the dispersion, and the formation of a nanoparticle film was confirmed based on electrode weight changes measured by a quartz crystal microbalance. Atomic force microscopy revealed that the resulting films were molecularly flat and homogeneously distributed across the electrode surface. Cyclic voltammetry (CV) curves of nanoparticle monolayers and typical nanoparticle aggregates are shown in Fig. 1. The reaction rates of metal sites, estimated from the oxidation peak areas, were 90% for the nanoparticle monolayers and 5% for the aggregates. These results demonstrate that the monolayer configuration maximizes the accessibility of catalytic metal sites. Nanoparticle monolayer films showed over 100-fold higher weight-normalized catalytic performance compared to the aggregates. Spectroscopic analysis elucidated that the structural reconstructions of the nanoparticles occurred during the electrochemical process, which contributed to the enhancement of intrinsic catalytic performance.

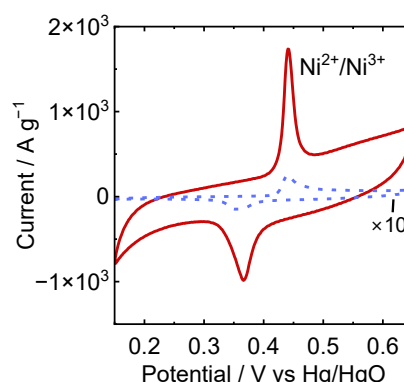


Fig. 1. CV curves of Ni-MHA nanoparticle monolayer film (solid line) and aggregate (dotted line).

1) Tarutani, N. *et al.*, *ACS Mater. Lett.*, **4**, 1430–1435, (2022).

Mizuki Sato¹, Daisuke Yoshioka¹, Yuki Nagai¹, and Yoichi Kobayashi¹

¹Ritsumeikan University

E-mail: sc0128hk@ed.ritsumei.ac.jp (Mizuki Sato),
ykobayas@fc.ritsumei.ac.jp (Yoichi Kobayashi)



Higher excited-state dynamics of perylene monoimide coordinated to inorganic nanocrystals

Higher excited states of organic molecules, which are accessed by further excitation of transient species, typically undergo rapid nonradiative relaxation to the lowest excited state. However, if ultrafast electron transfer can compete with this deactivation process, the high redox potentials associated with these higher excited states can be harnessed for advanced chemical transformations. We previously demonstrated ultrafast and efficient electron transfer from the higher excited states of perylene bisimides coordinated to cadmium sulfide nanocrystals.¹⁾ In this study, we synthesized a hybrid nanomaterial consisting of perylene monoimide (PMI) ligands coordinated to insulating hafnium oxide (HfO₂) nanocrystals (PMI-HfO) to further increase the reduction potential of higher excited states (Fig. 1a). We investigated the excited-state dynamics of PMI-HfO₂, including higher excited states, in detail using pump-probe spectroscopy and pump-push-probe spectroscopy (Fig. 1b).

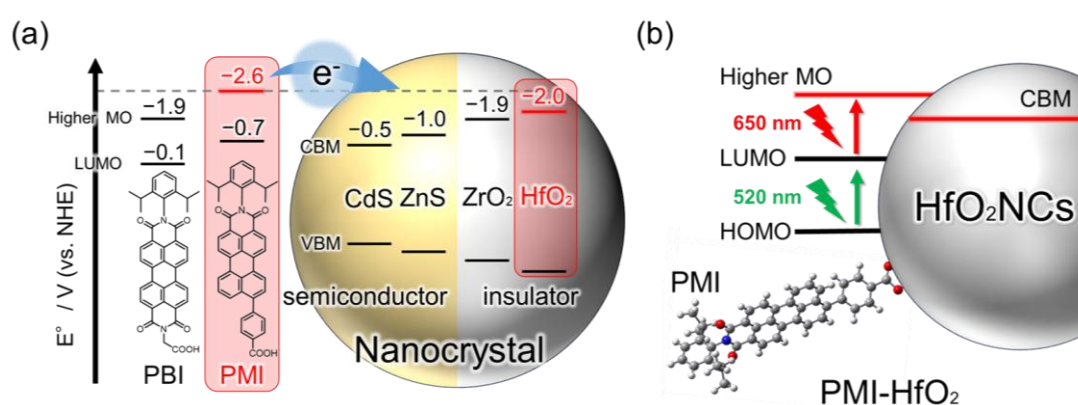


Fig. 1 (a) Schematic energy diagram of the organic ligands and nanocrystals. (b) Schematic illustration of higher excited state of PMI-HfO₂

1) Yoshioka, D., Fukuda, D., Kobayashi, Y., *Nanoscale*. **13**, 1823 (2021).

Kohki Tanaka, Yuki Nagai, and Yoichi Kobayashi

Affiliation

E-mail: sc0130hv@ed.ritsumei.ac.jp (Kohki Tanaka),
 ykobayas@fc.ritsumei.ac.jp (Yoichi Kobayashi)



Visible light-induced decomposition of perfluoroalkyl substances by CdS/ZnS core/shell nanocrystals

Perfluoroalkyl substances (PFASs), such as perfluorooctanesulfonic acid (PFOS), have been extensively used in various industries due to their exceptional chemical and thermal stability. However, their remarkable stabilities also result in severe environmental persistence, posing significant challenges for their degradation. In our previous study, we demonstrated efficient PFOS decomposition under visible-light irradiation using cadmium sulfide nanocrystals (CdS NCs). Nevertheless, the leaching of cadmium ions into aqueous solutions significantly hinders their practical application.

To overcome this limitation, we synthesized CdS/ZnS core/shell nanocrystals (CdS/ZnS NCs) and evaluated their photocatalytic performance under 405 nm LED light (616 mW/cm²). Although the ZnS shell slightly reduced the defluorination efficiency from 80.1% to 75.5% after 48 hours, it successfully suppressed Cd²⁺ leaching by 93.5%. While a small amount of Zn²⁺ leaching was still observed, the overall stability of the catalyst was substantially improved. These findings highlight the potential of CdS/ZnS NCs as an efficient and environmentally benign platform for PFAS degradation under mild aqueous conditions.

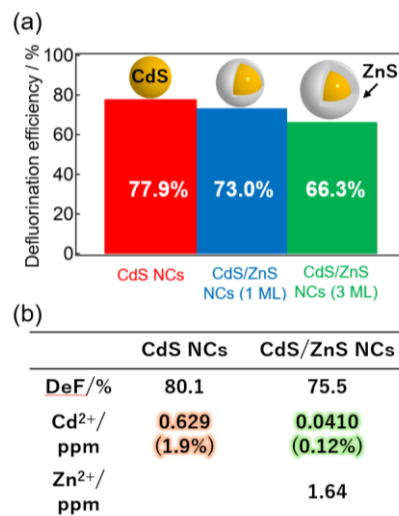

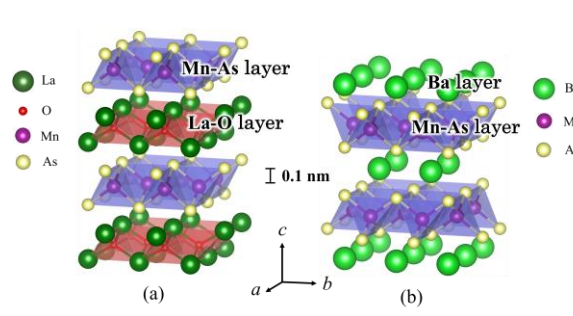
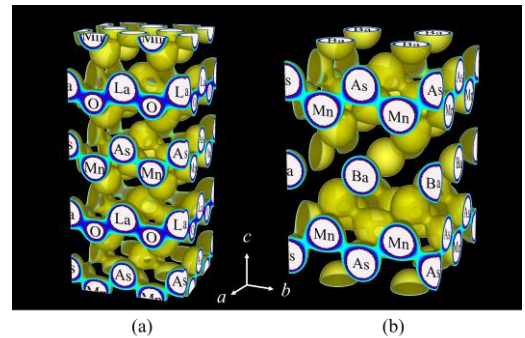


Fig. 1 (a) Defluorination efficiency of PFOS under 405 nm-light irradiation using CdS and CdS/ZnS NCs (1, 3 monolayers (ML)). (b) Leached ions after 48 hours of irradiation.

- 1) Y. Arima, Y. Okayasu, D. Yoshioka, Y. Nagai, Y. Kobayashi, *Angew. Chem. Int. Ed.* **63**, e202408687 (2024).

K. Katayama, C. Moriyoshi and K. Takase [†]		
Affiliation: Graduate school of advanced science and engineering, Hiroshima university, Japan		
[†] College of science and technology, Nihon university, Japan		
E-mail: kentaro-katayama@hiroshima-u.ac.jp (Kentaro Katayama)		
Electron density distribution analysis of Mn–As layered compounds with different types of antiferromagnet		
<p>Electron density analysis using high-efficiency synchrotron radiation X-ray diffraction (SXRD) data is widely used in materials science research. In this study, we employed this method to examine the antiferromagnetic layered compounds (LaO)MnAs and BaMn₂As₂ (Fig. 1). Both compounds have Mn–As layers with sub-nanometer interlayers. These materials have been regarded as Mott insulators from the 3d⁵ electronic configuration of Mn²⁺ ions. The Néel temperature is 360 K for (LaO)MnAs, while it is 625 K for BaMn₂As₂. To discuss the difference in the Néel temperature, we experimentally determined the electron density distribution $\rho(\mathbf{r})$ of the two compounds and investigated the ionic state of the constituent atoms.</p> <p>Figure 2 shows $\rho(\mathbf{r})$ of (LaO)MnAs and BaMn₂As₂. The valence of each layer was determined by integrating the $\rho(\mathbf{r})$ within that layer. The ideal ionic state of the Mn–As layer is -1, consisting of Mn²⁺ and As³⁻ ions. However, the ionization of the Mn–As layer in (LaO)MnAs was less complete than in BaMn₂As₂. This result suggests that the Mn ion in (LaO)MnAs cannot be fully described by a simple 3d⁵ model.</p>		
		
Fig. 1 Crystal structure. (a) LaOMnAs. (b) BaMn ₂ As ₂ .		Fig. 2 3D electron density map (isosurface level of 0.5e Å ^{–3}). (a) LaOMnAs. (b) BaMn ₂ As ₂ .

Kota Nakanishi, Chikako Moriyoshi, Shogo Kawaguchi and Ryo Sasai

Graduate school of advanced science and engineering, Hiroshima university, Japan

E-mail: m245767@hiroshima-u.ac.jp (Kota Nakanishi)



The effect of charge density on the crystal structure of layered double hydroxides of the Ni-Al type containing carbonate or chloride ions

The crystal structure of layered double hydroxides (LDHs) consists of alternating layers of octahedral metal hydroxide ($M^{2+}_{1-x}M^{3+}_x(\text{OH})_2$) and anions with water molecules ($A^{n-} \cdot m\text{H}_2\text{O}$). Hereafter, we will use the following convention for LDH: $A^{n-} M^{2+} M^{3+} (x)$. Crystal structure analysis is a powerful tool for understanding the characteristics of LDHs, such as the order of anion exchange [1]. This study aims to investigate how x , which controls the charge density, affects the crystal structure of $\text{CO}_3\text{-NiAl}(x)$ and $\text{Cl-NiAl}(x)$ ($x = 1/3, 1/5$). The X-ray diffraction data were obtained at BL13XU at SPring-8 and analyzed using the Rietveld method.

Figure 1 shows the crystal structure of LDH, as well as the thickness of the host layer (t) and the interlayer space (w). As x increased, the value of t increased and the value of w decreased, regardless of the type of anion species present between the layers. The largest t and the smallest w were observed in $\text{CO}_3\text{-NiAl}(1/3)$. These results suggest that, in the case of $\text{CO}_3\text{-NiAl}(x)$, there are interactions other than electrostatic ones between the positive charge of the host layer and the negative charge of the interlayer anions.

[1] R. Sasai *et al.*, *Bull. Chem. Soc. Jpn.* **2022**, 95, 802.

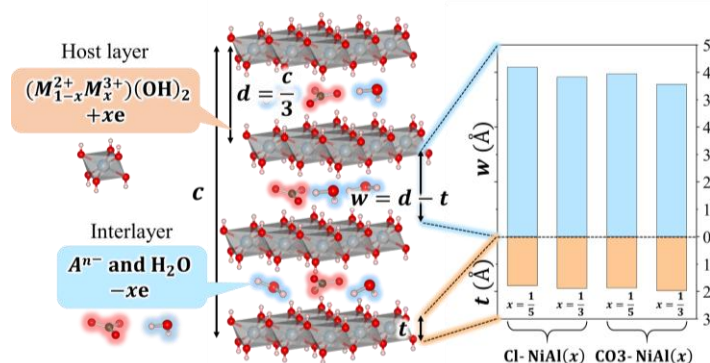

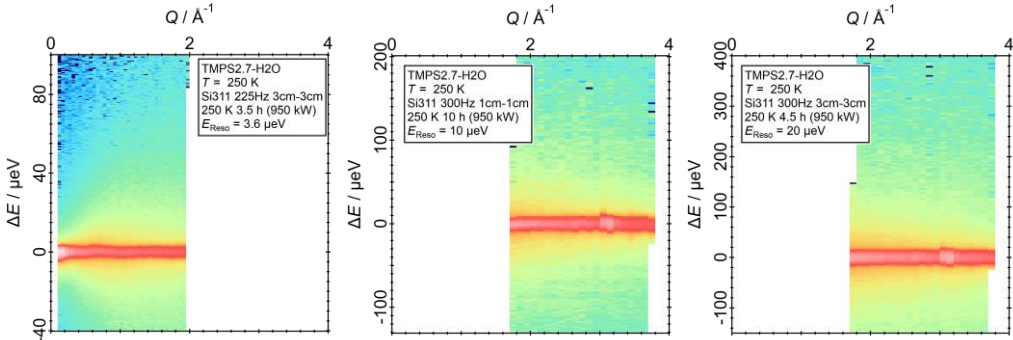


Fig. 1 Crystal structure of LDH, as well as the thickness of the host layer (t) and the interlayer space (w) of $\text{CO}_3\text{-NiAl}(x = 1/3, 1/5)$ and $\text{Cl-NiAl}(x = 1/3, 1/5)$. The values of t and w were calculated using the lattice parameter c and the z -coordinate of oxygen in the host layer.

Takeshi YAMADA		
Affiliation CROSS		
E-mail:t_yamada@cross.or.jp		
Title of the presentation		
QENS study on local dynamics of hydration water using Si311 analyzer		
<p>Water is an indispensable substance in our daily lives and is ubiquitous. Water in biomaterials and functional materials is closely related to their functions. These waters are hydrated with substances and confined in nanometer-sized spaces. Molecules confined in such nanospaces exhibit different structures and dynamics from those in the bulk due to interactions with molecules forming the space and size effects. Quasi-elastic neutron scattering (QENS) is suited to investigate the dynamics of hydrated water and/or bulk water at the molecular scale. Presenters have previously investigated the dynamics of water in phospholipid bilayers and in mesoporous silica pores, focusing on translational motion. On the other hand, the effect of restricted space on local modes such as rotational motion has not been well investigated.</p> <p>The objective of this study is to clarify local modes such as rotational motion of water molecules in restricted space using the Si311 analyzer of BL02-DNA in MLF J-PARC, which can measure high-Q regions with high energy resolution. Figures show the QENS profile of water in hydrophilic mesoporous silica (left (Si111 analyzer): energy resolution (EReso), 13 μeV , middle and right (Si311 analyzer) , EReso = 10μeV and 20 μeV, respectively). In the presentation, we will show the detailed fitting result.</p>		
		

Yoon Kang, Jae-Min Oh

Affiliation

E-mail: kgyoon0206@naver.com (Yoon Kang),
jaemin.oh@dongguk.edu (corresponding, Jae-Min Oh)



Title of the presentation

Trace blood detection by inducing fluorescence of hemoglobin
 via selective iron exclusion

This study proposes a method for detecting trace blood by selectively removing the central Fe from hemoglobin to induce fluorescence. In heme, Fe(II) or Fe(III) is coordinated to a porphyrin ring, and the resulting metal-to-ligand charge transfer (MLCT) promotes non-radiative decay of excited electrons, suppressing porphyrin's intrinsic fluorescence under UV light. To induce fluorescence, human whole blood was treated with chelate (oxalic acid) and reductant (ferrous sulfate) at 80 °C for 30 minutes. Oxalic acid chelated and removed the central iron ion from heme; ferrous ion reduced Fe^{3+} to Fe^{2+} to inhibit re-metalation, thereby promoting formation of fluorescent protoporphyrin IX. The generated protoporphyrin IX exhibited strong fluorescence under 395 nm UV irradiation, increasing proportionally with oxalic acid concentration. The fluorescence was most clearly visible to the naked eye at an oxalic acid to hemin (a heme substitute) mass ratio of 4500:1 and above 1 mol/L. Furthermore, we found that Fe exclusion and fluorescence generation in solution could be applied to latent bloodstain detection; oxalic acid paste was applied to dried artificial hemoglobin stains, enabling iron removal and fluorescence induction.

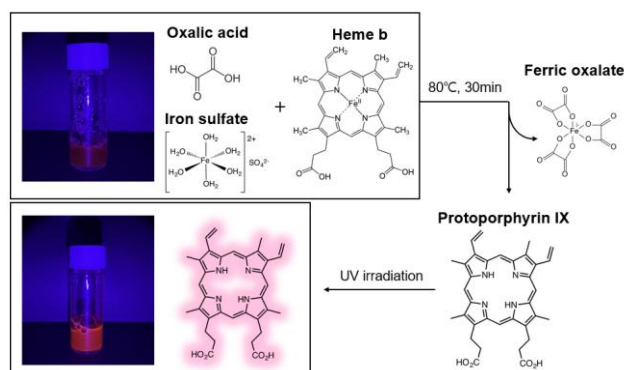

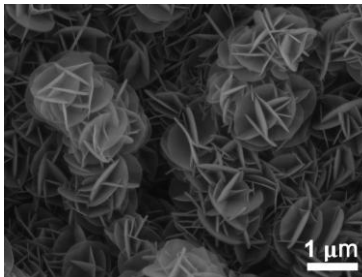



Figure 1. Mechanism of Fluorescence Induction via Iron Exclusion from Heme b in Hemoglobin

Taeho Kim ¹ , Yoon Kang ¹ , Jaeseong Kim ¹ , Rena Oi ² , Shota Mochizuki ² , Ryoto Kobayashi ² , Tomohiko Okada ^{2*} , and Jae-Min Oh ^{1*}		
Affiliation E-mail: taeho0408@naver.com (Taeho Kim), jaemin.oh@dongguk.edu (corresponding, if any)		
Title of the presentation Anisotropic growth of layered double hydroxides on planar aluminum or spherical alumina substrates		
<p>Anisotropic assembly of layered double hydroxides (LDH) flakes were directly obtained either on flat aluminum plates or spherical alumina balls via controlled surface crystal growth. The strategy relies on controlled release of trivalent aluminum ions from the substrate, enabling in-situ crystallize into LDH sheets on the surface. On planar aluminum plate, LDH nanosheets were found to grow in a vertical alignment upon reaction with Mg²⁺ divalent cations, OH⁻ anions and substrate-derived Al³⁺ trivalent cations. The calcination and rehydration, so called, reconstruction dramatically increased surface roughness of vertically grown LDH to generate lotus-effect hydrophobicity. In order to grow LDH on spherical alumina, the surface was pretreated with alkaline solution to create nucleation sites. Subsequent urea-assisted hydrothermal synthesis under the presence of Mg²⁺ source produced uniform LDH coverage with sand-rose architectures. Scanning electron microscopy and energy-dispersive X-ray spectroscopy validated the formation of randomly arranged LDH nanosheets on both planar aluminum substrate and uniform sand-rose LDH structures on spherical alumina balls. These results confirmed that controlled surface crystal growth yields distinct anisotropic LDH coatings on both substrate types.</p>		
 		<p>Figure 1. Scanning electron microscopy images of LDHs on Al plate and alumina balls</p>

Shota Mochizuki	
Shota Mochizuki ¹⁾ , Tomohiko Okada ¹⁾ 1) Graduate School of Science and Technology, Shinshu University E-mail: 25w1056f@shinshu-u.ac.jp (Shota Mochizuki), tomohiko@shinshu-u.ac.jp (Tomohiko Okada)	
Hybridization of a Zn-smectite with spherical silica particles	

Spherical plastic beads have been used in cosmetics to scatter light and blur skin imperfections, however non-biodegradability concerns marine pollution. As an alternative, this study explores the use of naturally abundant silica. A white cosmetic pigment has been developed by directly growing layered Zn-substituted hectorite on spherical silica particle to enhance light multiple scattering, and to mimic optical properties of a white beetle comprising anisotropic fibrous chitin¹⁾.

The synthesis involved using porous (FB-82) and non-porous (KE-P250) silica supports with the size of a few micrometers. After silica powder was mixed into an aqueous LiF, ZnCl₂, and urea solution in controlled molar ratios, the mixture was treated at 80°C for 48 h, followed by washing and subsequent drying.

Diffraction peaks in the XRD pattern were characteristic of hectorite in all samples. When non-porous silica was used, Zn(OH)F coprecipitated due to insufficient dissolved silica during the heat treatment in the aqueous alkaline media. In contrast, porous silica provided Zn-hectorite without formation of Zn(OH)F. SEM images revealed hemispherical aggregates (0.1–0.2 μm) on the porous silica, which were composed of plate-shaped particles. The size of the particulate plates became larger when the non-porous silica was used, indicating that specific surface area of silica determines the final crystalline size and its aggregate.

1) Burrese, M., et al., *Sci. Rep.*, **4**, 6075 (2014).

Rena Oi

Rena Oi¹⁾, Tomohiko Okada¹⁾

1) Graduate School of Science and Technology, Shinshu University

E-mail: 24w1007d@shinshu-u.ac.jp (Rena Oi),

tomohiko@shinshu-u.ac.jp (Tomohiko Okada)




Adsorption of Anionic Red Dyes on Smectite in the Presence of Multivalent Cations

Photodegrading of red dyes is a practical issue in makeup cosmetics. Maya Blue comprising indigo and clay minerals is an excellent durability against light and heat. Improving photostability of a cationic red dye has been investigated using a cation-exchangeable layered silicate¹⁾. Designated colors for cosmetics are generally anionic dyes, thereby, we aim to improve photostability of an anionic red 201 dye (Lithol Rubin BK: abbreviated as BK hereafter). Because the layered silicate (Kunipia-F, abbreviated as KF hereafter) is negatively charged, we examined to using multivalent cations (Ca^{2+} and Al^{3+}) as a connector for immobilizing BK.

Homoionic Ca^{2+} - and Al^{3+} -exchanged KFs (KF-Ca and KF-Al) were allowed to react with 0.12 mmol BK in the presence of CaCl_2 and $\text{AlCl}_3 \cdot 6\text{H}_2\text{O}$ under magnetic stirring, followed by drying to obtain KF-Ca_BK and KF-Al_BK samples, respectively. After the dried samples were irradiated with a UV lamp for 20 days, the color difference ΔE^* was obtained from the UV-Vis reflectance spectrum to evaluate photostability.

Intercalation of BK into KF-Al was confirmed by XRD; two broad diffraction peaks ($d_{001} = 2.0$ and 1.6 nm) were located at a lower 2θ region of the pristine KF-Al ($d_{001} = 1.4$ nm), whereas a negligible shift of the (001) plane was observed for KF-Ca with emerging diffraction due to a calcium salt of BK at $2\theta = 4.8^\circ$. This suggests coordination of BK with Ca^{2+} in solution and interaction with Al^{3+} in KF-Al, where the Ca salts would crystallize at the external surface of KF-Ca. The BK content estimated by TG-DTA in KF-Ca_BK was comparable to that in KF-Al_BK. The photostability of KF-Ca_BK based on ΔE^* (2.3) was improved to 0.36 for KF-Al_BK, suggesting that intercalation of BK into KF-Al played an important role in the photostabilization.

1)A.P.Teepakakorn, et al., *Langmuir*, **34**, 14069 (2018).

Kakeru Taniuchi	
Kakeru taniuchi ¹⁾ , Tomohiko Okada ¹⁾ , Masashi Morita ²⁾ 1)Graduated School of Science and Technology, Shinshu University 2)Tokyo University of Agriculture and Technology E-mail: 24w1028g@shinshu-u.ac.jp (Kakeru Taniuchi), tomohiko@shinshu-u.ac.jp (Tomohiko Okada), m-morita@go.tuat.ac.jp (Masashi Morita)	
Formation of Titania Particles via Incorporation of Titanium (IV) Oxyacetylacetonate into Mesoporous Silica	

Amorphous titania is useful substance in applications as UV absorber. Controlling morphology of the particle is limited because of its instability. It has been reported that the morphology of anatase particles was controlled using nanopores in a mesoporous silica.¹⁾ However, there is no report on the morphology control of amorphous titania. We report that size of the particles is reflected from pore diameters of SBA-15 using titanium (IV) oxyacetylacetonate (TiO(acac)₂). We also study that surface density of silanol groups on SBA-15 affects a structure of titania particle.

SBA-15s with pore diameters of 8 and 18 nm were prepared according to a previously reported method.²⁾ After impregnation into a methanol solution of TiO(acac)₂ at a Ti/Si ratio of 1/5, the products were calcined at 1000°C. Surface density of the silanol groups was increased by reacting aq. HCl at 100° C for 24 h.

Based on XRD analysis, anatase crystals were formed with the size of approximately 20 nm, when the original SBA-15s were used. On the other hand, no diffraction due to anatase was observed, when using acid-treated SBA-15 (8 nm). The particles observed in TEM images were same size as the pore diameter without lattice fringe of TiO₂. Pore diameter and surface density of silanol groups on SBA-15 were dominant factors in determining the crystallinity and the particle size of final titania; particle growth and crystallization to anatase were restricted on the silanol groups with a higher density in 8 nm of the pore diameter.

1) K. Vibulyaseak, et al., *Langmuir*, **33**, 13598 (2018); 2) M. Sohmiya, et al., *Nanoscale Adv.*, **1**, 1726 (2019).